Nanoscale

Accepted Manuscript

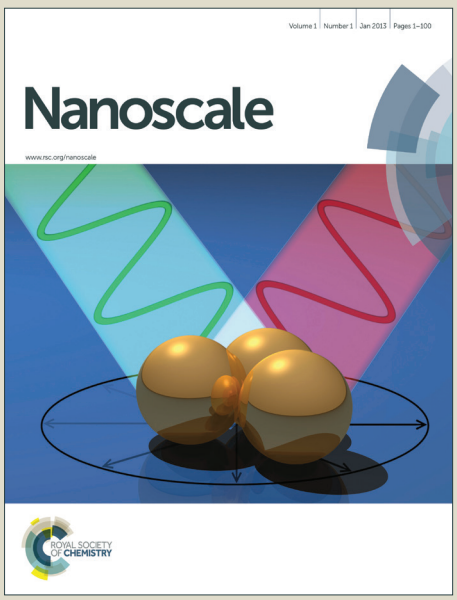

ROYAL SOCIETY OF CHEMISTRY

www.rsc.org/nanoscale

From Monomer to Monolayer: a Global Optimisation Study of $(ZnO)_n$ Nanoclusters on the Ag Surface

Ilker Demiroglu[1], Scott M. Woodley[2], Alexey Sokol[2], Stefan T. Bromley*[1,3]

[1] *Departament de Química Física and Institut de Química Teòrica i Computacional, Universitat de Barcelona (IQTCUB), E-08028 Barcelona, Spain*

[2] *University College London, Kathleen Lonsdale Materials Chemistry, Department of Chemistry, 20 Gordon Street, London WC1H 0AJ, United Kingdom*

[3] *Institució Catalana de Recerca i Estudis Avançats (ICREA), 08010 Barcelona, Spain*

* Corresponding author: s.bromley@ub.edu

Abstract

We employ global optimisation to investigate how increasingly sized oxide nanoclusters can best adapt their structure to lower the system energy when interacting with a realistic extended metal support. Specifically, we focus on the (ZnO)@Ag(111) system where experiment has shown that the infinite Ag(111)-supported ZnO monolayer limit corresponds to an epitaxially 7:8 matched graphene-like (Zn_3O_3)-based hexagonal sheet. Using a two-stage search method based on classical interatomic potentials and then on more accurate density functional theory, we report global minina candidate structures for Ag-supported $(ZnO)_n$ cluster with sizes ranging from n=1-24. Comparison with the respective global minina structure of free space $(ZnO)_n$ clusters reveals that the surface interaction plays a decisive role in determining the lowest energy Ag-supported $(ZnO)_n$ cluster structures. Whereas free space $(ZnO)_n$ clusters prefer to adopt cage-like bubble structures as they grow larger, Ag-supported $(ZnO)_n$ clusters rapidly become progressively more like planar cuts from the infinite graphene-like ZnO single monolayer with increasingly size. This energetic favourability for planar hexagonal Ag-supported clusters over their 3D counterparts can be partly rationalised by the ZnO-Ag(111) epitaxial matching and the increased number of close interactions with the Ag surface. Detailed analysis shows that this tendency can also be largely attributed to the capacity of 2D clusters to structurally distort to improve their interaction with

the Ag surface relative to more rigid 3D bubble cluster isomers. For the larger sized clusters we find that the adsorption energies and most stable structural types appear to be rather converged confirming that our study makes a bridge between the Ag-supported ZnO monomer and the infinite Ag-supported ZnO monolayer.

Introduction

Nanosized clusters typically containing a few tens of atoms, although often difficult to study in microscopic detail by experiment alone, have been widely investigated by computational modelling.[1,2,3] In the large majority of these theoretical studies the nanoclusters in question are of metals or inorganic materials and are treated as isolated species in free space. In real world applications, however, such nanoclusters are either on or within a supporting macroscopic material (e.g. heterogeneous catalysts, nanocomposites). In such cases it is often the metal-inorganic interface interaction that is important, with the oxide-supported metal nanocluster system being particularly heavily studied.[4] In detailed atomistic modelling of this system, in order to assess accurately the effect of the nanocluster-support interaction on the structure of the nanoclusters, recent work has employed global optimization algorithms to search for the most energetically stable supported nanoclusters.[5,6] Importantly, these latter studies take into account the interaction with the support during the global optimization searches (i.e. as opposed to searching for low energy nanocluster isomers in free space and then placing them on the support). This approach is particularly important when large structural changes in the metal nanocluster are induced by the oxide support and when energy ranking of the isomers in free space and on the surface differs dramatically. In the present investigation we also employ this powerful approach for studying nanoscale metal-inorganic interactions, but in the far less studied case of metal-supported oxide nanoclusters. Specifically, we consider the case of zinc oxide (ZnO) nanoclusters supported on the surface of silver.

ZnO is an important semiconductor which, due to its remarkable optical and electronic properties, is already widely used and has great promise at the nanoscale in a range of new device applications (e.g. gas sensors, optoelectronic devices, and photocatalysis).[7] Although the structures and properties of small free space $(ZnO)_n$ nanoclusters have been studied by classical atomistic and quantum electronic structure calculations by a number of groups,[8-13] there is relatively little theoretical work on the interaction of nano-ZnO with a support. We note that this situation lies in stark contrast to the abundant theoretical literature on oxidation processes at transition metal surfaces.[14,15] Following the

importance of the ZnO/Ag interface in optical coatings for solar control windows,[16,17] a few groups have used electronic structure calculations to study the bulk ZnO-Ag interface.[18-21] Belbruno *et al*. have modeled $(ZnO)_n$ clusters, with $n \leq 3$, supported on MgO(001)[22] and, with $n \leq 4$, on graphite[23] surfaces, but, as far as we are aware, only one theoretical study has looked at Ag(111)-supported $(ZnO)_n$ for very small $n \leq 3$ species.[24] In the size range between these Ag-supported sub-nanoscale molecular ZnO clusters and ZnO-Ag interfaced bulk films, a number of interesting Ag-supported nano-ZnO systems have been prepared experimentally. Ag-supported ZnO nanorods with diameters as small as 15-30 nm, for example, display a strong growth dependence on the crystallographic orientation of the Ag surface.[25] These systems have further been shown to be more photocatalytically active than pure ZnO nanorods, implying that the Ag-(nano)ZnO interface helps promote the separation of photo-generated electron-hole pairs.[26] Smaller nanometer sized gas phase ZnO clusters have also been deposited on Au(111) surfaces showing band structure quantization.[27] Moving towards more two-dimensional (2D) systems, extremely thin films of ZnO on Ag(111) have been carefully prepared and characterized by surface science techniques.[28] Interestingly, when such ZnO nanofilms are less than four monolayers thick they exhibit a non-bulk-like layered "graphitic" phase of flat sheets, each based on tessellated hexagonal $(ZnO)_3$ units. It is notable that this phenomenon was first predicted using electronic structure for free-standing thin ZnO films.[29] More recently, we have also similarly modelled the interaction of a single graphene-like monolayer of this layered ZnO nanophase with the Ag(111) surface.[30]

The present work significantly extends on previous computational modelling of Ag-supported very small $n = 1\text{-}3$, $(ZnO)_n$ molecular species[24] to systematically study $(ZnO)_n$ clusters, both interacting with a Ag(111) support and in free space, up to a size of $n = 24$. Our investigation into how ZnO nanoclusters preferentially adsorb on a metal surface provides valuable insight into the initial stages of ZnO thin film growth, thus helping to bridge the gap between the metal-supported ZnO monomer and the metal-supported ZnO monolayer. Sheet-like 2D $(ZnO)_n$ cluster isomers resembling the infinite Ag-supported ZnO monolayer are not found to compete in energy with the cage-like isomers in free space. Conversely, our global optimization calculations for Ag-supported $(ZnO)_n$ clusters show that there is a complex competition between the energetics of intra-cluster Zn-O bonding, tending to favour closed cage-like clusters in free-space, and the Ag-ZnO metal-cluster interaction, which encourages flatter sheet-like clusters, or wetting. This competition tends to result in more 2D ZnO_n clusters being preferred when interacting with the Ag(111) surface, in line with the known tendency of ZnO to form infinite 2D sheets up to coverages of 2-3 monolayers on Ag(111).[28]

In addition to being a thorough, atomically detailed examination of ZnO nanoclusters on Ag(111), and thus being of relevance to a number of experimental studies (see above), our work more generally provides a novel example of how global optimization can be extended to examine the interaction and growth of clusters of inorganic materials on a support.

Methodology

Throughout this study we have modelled the Ag-supported $(ZnO)_n$ nanoclusters with two complementary approaches: in stage 1, classically, using interatomic potential (IPs); and, in stage 2, through density functional theory (DFT) based *ab initio* calculations. Due to the high computational cost of the latter, IPs were first employed during the extensive global optimization searches of the configurational energy landscape of both free-space and Ag-supported $(ZnO)_n$ cluster structures. The IPs employed included ZnO IPs developed by Whitmore *et al*.[31] to study ZnO surface structures, and those developed for the Ag–Zn and Ag–O interactions between ZnO clusters and the Ag surface[32]. For the global optimisation searches we employed a Monte Carlo Basin Hopping (MCBH) approach,[33] which has been recently implemented into the Knowledge-Led Master Controller (KLMC)[34,35,36] code that also utilizes the different analytical forms of IPs available in and the local minimization routines of the General Utility Lattice Program (GULP).[37] For this study, KLMC has been extended, in particular, to enable the global optimization of the atomic structure for a cluster in the presence of a surface. We performed MCBH searches over the IP energy landscapes of $(ZnO)_n$ nanoclusters in free space and on a Ag support for all sizes between n = 1 and 16, and two larger sizes n = 21 and 24. In the first stage, the Ag surface unit cells include either two 64-atom layers (for n = 1 and 12) or two 120-atom layers (for the larger sized ZnO nanoclusters) constrained to their bulk positions. Initial Zn and O positions are random, but nonetheless constrained to a spherical region in free space or hemi-spherical region above the Ag surface with the minimum interatomic distance greater than 80% of a typical Zn-O bond length. Additional scans of the predicted free-space cluster structures over the Ag surfaces were also performed, using KLMC, in which the MC steps changed both the initial position and orientation of each nanocluster rather than each individual Zn and O atom. Note that for each trial configuration, the atomic structure of the nanocluster was fully relaxed by KLMC via two calls to one of GULP's local optimization routines. In the first call to GULP, a rigid ion model with formal charges is employed; the relaxed structure is subsequently refined during the second call, in which the polarisable shell model is employed. This double minimisation approach has the benefit of being more robust (the shell model can fail if the

polarization of oxygen anions is too extreme, as can happen for initial structures that are far from equilibrium) and efficient (the shell model has six, rather than three, variables for each oxygen anion).

To find the global minimum (GM) and other low-energy local minima (LM) structures, as defined by DFT, a selection of the best IP candidate structures for each cluster size (including the GM and typically 15-20 LM) were refined in a second, DFT stage. Here, we employed the PW91 generalized gradient approximation (GGA) exchange-correlation density functional[38] as implemented in the VASP code[39]. The projector augmented wave approach[40,41] was used to describe the effect of core electrons on the valence states. Valence states were taken as $d^{10}s^2$, s^2p^4 and $d^{10}s^1$ for Zn, O and Ag atoms, respectively. One-electron valence states were expanded in a plane wave basis up to a kinetic energy cut-off of 400 eV for which the total energy is converged to within 0.03 eV.

The Ag surface models were constructed from the DFT optimized bulk structure. The lattice constant of the Ag bulk unit cell was found to be 4.15 Å, which is very close to a previous theoretical result[42] of 4.17 Å, and slightly higher than the experimental value[43] of 4.09 Å. The Ag(111) surfaces were modeled using a four-layered slab cut from the bulk, where only the bottom layer of atoms were constrained to their bulk positions during relaxation. The initial Zn and O atom positions were taken from our IP results obtained in stage one. Large surface supercells of the Ag support were chosen in order to keep the supported ZnO clusters ≥ 1nm apart, thus eliminating, or at least reducing, spurious interactions between the nanoclusters and their periodic images. Specifically, a $(8 \times 4\sqrt{3})$ Ag supercell was used for the smaller sized $(ZnO)_n$ clusters ($n \leq 16$) and a $(9 \times 5\sqrt{3})$ Ag supercell for larger cluster sizes. Due to the very large number of calculations and the large size of the periodic systems, the DFT calculations were performed using only the Γ point in reciprocal space. In all cases the remaining atomic positions were optimized until the forces on the atoms became less than 0.02 eV/Å. Using a slightly thicker Ag slab and a more stringent convergence criteria did not change the ranking (based on energy) or the essential structural features. All results reported below, energies and atomic structures, are taken after the completion of stage two, *i.e.* only DFT energies and DFT refined structures are presented in the figures.

Previous GGA calculations on a full ZnO monolayer supported on Ag(111) have shown that the interaction between metal and oxide is fairly weak (0.14-0.17 eV/ZnO)[32, 44] and likely of mainly electrostatic origin. Although the interaction strength between the sheet and the Ag support is increased with the addition of extra *ad hoc* dispersive forces introduced via empirically parameterized two-body interaction terms,[32] it is not clear that such a procedure is necessary, or in any sense "corrective" in this case. Other work has shown, for example, that adding such two-body dispersive terms to pure GA DFT

calculations significantly overestimates binding energies with the Ag(111) surface of both organic molecules[45] and 2D BN sheets[46,47] compared to experiment. Our previous calculations also showed no evidence of significant charge transfer or covalent bonding between the Ag(111) surface and the supported infinite 2D-ZnO sheet, with both having almost indistinguishable atomically partitioned charges in isolation and in the combined system.[32] This electrostatic but non-charge transferred interaction is also confirmed by GGA DFT+U calculations which indirectly open the O 2p – Zn 4s bandgap in the Ag(111)-supported ZnO monolayer through addition of a large onsite Hubbard U term to the Zn 3d states, but where the oxide-metal binding energy from standard GGA DFT calculations is found to be hardly perturbed.[44] Considering the above, we believe that our pure GGA based DFT approach should provide a adequately accurate description of ZnO clusters on Ag(111).

The total energies of the relaxed $(ZnO)_n$ nanoclusters in free space are denoted as $E_n^{free\ space}$. To compare these free-space total energies with those of Ag-adsorbed $(ZnO)_n$ clusters, the energies of the Ag-supported clusters, $E_n^{on\ surface}$, are defined as the total system energy of the Ag-supported cluster system, E_n^{tot}, minus the energy of an isolated relaxed Ag slab, E_{Ag_slab}. We define the adsorption energy of each $(ZnO)_n$ cluster with the Ag surface per ZnO unit, E_n^{ads}, as the difference in energy between the total system energy, and the sum of the total energy of the same cluster relaxed in free space and the total energy of the relaxed Ag slab (*i.e.* $E_n^{ads} = (E_n^{tot} - (E_n^{free\ space} + E_{Ag\_slab}))$. We note that the total system energy can be defined as a sum of three terms: $E_n^{tot} = E_n^{ads} + E_n^{free\ space} + E_{Ag\_slab}$, where the last term is a constant. The surface-induced distortion for each $(ZnO)_n$ cluster, $E_n^{surf\ distort}$, is defined as the difference in energy between the relaxed free-space cluster and the energy of the cluster in free space with a structure fixed at the Ag-adsorbed optimized geometry (*i.e.* $E_n^{surf\ distort} = E_n^{free\ space(ads)} - E_n^{free\ space}$). We also define the adsorption energy of a cluster with respect to the cluster in free space with the surface adsorbed geometry, $E_n^{ads(ads)}$, as the difference between the total energy and sum of the energy of the cluster in free space with a structure fixed at the Ag-adsorbed optimized geometry and the relaxed Ag slab (i.e. $E_n^{ads(ads)} = E_n^{tot} - (E_n^{free\ space(ads)} + E_{Ag_{slab}})$). From these definitions we can simply derive that: $E_n^{ads} = E_n^{surf\ distort} + E_n^{ads(ads)}$. It should also be noted that the clusters may have different orientations on the surface, which also changes their adsorption energies. In all cases we report data for the $(ZnO)_n$ cluster orientation with the highest E_n^{ads} found. All energies are normalized with respect to the number of ZnO units in the respective $(ZnO)_n$ cluster in order to compare systems with $(ZnO)_n$ clusters of different sizes. The meaning of each energy term and their inter-relations are summarized graphically in Fig. 1.

Results and Discussion

After briefly summarizing what is known from previous work about small free-space ZnO nanoclusters, we present our results on the ZnO nanoclusters in the presence of the Ag(111) surface for differently sized $(ZnO)_n$ clusters n = 1-16, 20, and 24. Finally, we present a few preliminary results exploring the effect of the surface morphology of the metal support on the supported ZnO nanoclusters.

Free Space $(ZnO)_n$ Clusters

According to their common structural features, the free space ZnO nanoclusters we find can be divided into families which we refer to as: sticks, rings, 2D clusters, and 3d clusters (or bubbles). Sticks are composed of one atom thick 1D chains of alternating Zn and O atoms, which can form rings by bending in order to connect their ends. The fusion of multiple rings can result in clusters of planar 2D clusters. The bending of these 2D patchworks can yield 3D tubes, if the ends are left open, or 3D cage-like bubble clusters, if completely closed. Multilayer spheroids, or nested bubbles found for larger cluster sizes than considered herein, are often referred to as onions in the literature. The coordination number of the atoms in these clusters depends both on the dimensionality of the structure and the position of the constituent ion in the structure (*e.g.* whether it is at an internal or an terminal site). Typically, the coordination number is two for 1D clusters, three for 2D clusters and four for 3D nanostructures for the internal ions, while it is often decreased by one in each case for the terminating ions. According to previous studies of isolated ZnO nanoclusters,[35,48] ring structures are stable up to $(ZnO)_7$, after which, on size increase, there occurs switch to bubble clusters that are more favourable in energy. This structural crossover has recently been confirmed for ZnO cluster anions in a cluster beam experiment[49] where the potential for bubble clusters to act as building blocks for cluster assembled bulk materials was highlighted.[50,51] Neither bulk-like wurtzite nor structures related to the extended polymorphic phases of zinc blende or rocksalt have been found to be stable for small sized nanoclusters. However, it has been estimated that the crossover from bubble structures (via nested bubbles) to denser, more bulk-like structures will take place at an approximate cluster size of $(ZnO)_{120}$.[52]

Through comparison with a previous global optimization study of free space ZnO nanoclusters by Al-Sunaidi *et al*[11], we find that the low-energy LM free-space nanoclusters were readily reproduced by the KLMC code.

Ag(111)-supported $(ZnO)_n$ clusters, n =1-4

In general, the possible atomic adsorption locations on the Ag(111) surfaces are the symmetry unique sites: on-top (T), above a single metal atom; bridge site (B), between two metal atoms; and hollow site (H), where higher coordination is possible (see Fig. 2). For the simple Ag(111)-supported ZnO monomeric stick, both atoms are above hollow site positions with a tilted orientation such that the O atom lies closer (1.61 Å) to the Ag surface plane than the Zn atom (2.00 Å). In free space, the DFT calculations confirm that the linear stick structures are less stable than the rings for n = 2 and 3, with energy differences of 0.35 and 0.92 eV/ZnO, respectively. However, on the support, the linear sticks become more stable than the rings with energy differences of 0.35 eV/ZnO for n = 2 and 0.11 eV/ZnO for n = 3. These results are also in line with the previous work of Bristowe *et al.*[24] who studied $(ZnO)_n$ adsorption on Ag(111) for n = 1-3 using DFT. The plane of the flat $(ZnO)_2$ four-membered ring, the centre of which is above an on-top position, lies parallel to the Ag surface (heights of the atoms above the surface plane are 1.92 and 1.95 Å for Zn atoms and 1.97 and 2.04 Å for O atoms). The $(ZnO)_2$ ring is oriented so that the O atoms are above bridge sites and the Zn atoms above hollow sites. The Ag atoms nearest the O atoms of the $(ZnO)_2$ ring also move 0.26 Å outwards (*i.e.* towards the ring) and the Ag surface atom below the ring centre moves 0.36 Å inwards (*i.e.* towards inner layers of the slab) while the other surface Ag atoms exhibit maximum displacements of 0.05 Å. A similar planar on-top adsorption geometry is also found for the $(ZnO)_3$ ring, which is slightly further (by ~0.2 Å) from the Ag-surface plane. As for the $(ZnO)_2$ ring, Ag surface distortions are also predicted near the $(ZnO)_3$ nanocluster; the surface Ag atom nearest the centre of the $(ZnO)_3$ ring moves 0.22 Å inwards, while two of the Ag surface atoms closest to two of the O atoms (see Fig. 2) move 0.09 Å outwards. The remaining Ag surface atoms exhibit maximum displacements of 0.03 Å from the surface plane. For the $(ZnO)_2$ and $(ZnO)_3$ stick structures, the nanoclusters retain their linear O-Zn-O configurations as in free space but bend about the more polarizable O atoms. Furthermore, the O atoms closest to on-top sites of the Ag surface move slightly away from the surface. As for the ZnO monomer, we note that the terminal oxygen atoms of the $(ZnO)_2$ and $(ZnO)_3$ sticks are situated above hollow sites and are considerably closer to the Ag surface plane (1.53 Å and 1.62 Å respectively) than the other atoms of the cluster (>1.95 Å). For n = 4, an 8-membered ring structure is predicted to be the GM both in free-space and on the surface. A 1D stick configuration for size n = 4 was found to be only 0.01 eV/ZnO higher in energy than the ring isomer when stabilized by the surface. Although these isomers are close in energy, considering the trend from n = 2-4, that the Ag-supported ring structures become more stable while the Ag-supported sticks become less stable as the

size increases (see $E_n^{on\ surface}$ values in Fig. 2), no 1D isomer is expected to be a global minimum $(ZnO)_n$ structure for $n > 4$.

In terms of E_n^{ads} with n increasing, the strength of interaction between the GM clusters and the Ag surface decreases rapidly from -2.95 eV/ZnO for the ZnO monomer to -0.34 eV/ZnO for the $(ZnO)_4$ ring. The relatively high adsorption strength of the monomer, and the other linear stick isomers for n = 2-4 (E_n^{ads}< -1.31 eV/ZnO in all cases), appears to be associated with charge transfer from the Ag support to the relatively close singly coordinated terminal Zn atom in each case (~0.5 e^- estimated from Bader atom partitioned charges[53]). For the n = 4 GM ring isomer, the computed Bader partitioned charges indicate that some charge transfer to the doubly coordinated Zn atoms also occurs, but is less (0.29 e^- / 0.07 e^- per Zn atom) than for the stick isomers. For all larger sized $(ZnO)_n$ nanoclusters ($n > 4$) considered below, all Zn atoms are either 2- or 3-coordinated and the charge transfer per Zn atom, as estimated by Bader charge partitioning, reduces with size (0.04-0.05 e^- per Zn atom at a cluster size of n = 24). Charge transfer is always found to be proportionally higher for the peripheral 2-coordinated Zn atoms on the planar clusters, which is concomitant with them tending to be closest to the Ag surface (see next section). For 3-coordinated Zn atoms the calculated Bader charge transfer is always relatively less. In the case of the limit of the Ag-supported infinite ZnO sheet, for example, where all Zn and O atoms are 3-coordinated, the Zn and O atoms are 2.8 Å above the Ag(111) surface and there is a negligible calculated charge transfer (0.025 e^-) per Zn atom. As atomic charge is not an observable, the numerical values given by atomic charge partitioning analysis, such as the Bader method used herein, are biased by the choice of the partitioning method employed. As such, although the above values should reflect tendencies of charge from the Ag support to move to, or to strongly polarise towards, the Zn atoms of the clusters with respect to cluster size and structure, they should not be taken as quantitative measures.

Ag(111)-supported $(ZnO)_n$ clusters, n =5-16, 20, 24

In agreement with previous studies for free-space $(ZnO)_n$ clusters, the GM candidates are found to be rings up to n = 7 and for sizes thereafter 3D cage-like bubble clusters dominate the low-energy isomer spectra. These free space GM isomer candidates are shown in Fig. 3. For $(ZnO)_n$ cluster sizes $n > 12$, free space bubble clusters are so much lower in energy than 2D clusters that the latter hardly appear in the lower energy range of the free-space global optimization searches. Such is the energetic dominance of

3D free space clusters for $n > 7$, in order to help to find possible low-energy free-space 2D cluster candidates in this size range, we had to supplement the set of 2D clusters found in our free space searches with 2D clusters found in the Ag-supported global optimization calculations. In global optimizations of the Ag-adsorbed $(ZnO)_n$ clusters, however, for all $n \geq 4$ cluster sizes studied here, we were always able to find a 2D cluster GM. This finding can be rationalized to an extent for $(ZnO)_n$ clusters with sizes n = 4-7 by the fact that 2D ring isomers are the free-space GM structures. We note, however, that the lowest energy 2D clusters in free space are generally not the lowest energy 2D configuration once adsorbed on the Ag surface. In fact, the only exceptions are found for $n < 6$, which are single rings.

In Fig. 4a-c we show plots of $E_n^{free\ space}$ and $E_n^{on\ surface}$ for the eleven $(ZnO)_n$ cluster isomers found with the lowest (*i.e.* most negative) $E_n^{on\ surface}$ values for cluster sizes n = 8, 12, and 16. In all three plots there is little variation in the $E_n^{on\ surface}$ values throughout the eleven isomers. In Fig. 4a the $E_n^{free\ space}$ values for size n = 8 also all lie in a similar narrow range of values with neither 2D nor 3D clusters being generally more stable. We note here that the least stable free space $(ZnO)_n$ cluster (of the eleven plotted) turns out to be the most stable Ag-supported cluster (*i.e.* lowest $E_n^{on\ surface}$ value). For size n = 12 in Fig. 4b we start to see a tendency for the 2D free space $(ZnO)_n$ clusters to be less stable than free space 3D clusters. For n = 16, in Fig. 4c, this trend results in a clear separation between the $E_n^{free\ space}$ values of the more stable 3D free space clusters with respect to those of the less stable 2D free space clusters.

For $n \geq 8$, the higher energetic stability of Ag-supported 2D clusters can be partially explained by their significantly more negative E_n^{ads} values with respect to 3D bubble clusters with increasing size. This, in turn, can be rationalized by the relatively higher number of close Ag-cluster atomic interactions in a supported sheet-like 2D $(ZnO)_n$ cluster with respect to a more cage like $(ZnO)_n$ cluster. Clearly, however, there is also trade-off between the energetic stabilization due to the adsorption on the surface and the energy destabilization in distorting away from the relaxed free space geometry to improve the interaction with the surface. Stated more formally, we recall from above that the magnitude of E_n^{ads} can be partitioned into a sum of two terms related to distortion and adsorption (*i.e.* $E_n^{ads} = E_n^{surf-distort} + E_n^{ads(ads)}$). In Fig. 5 we plot E_n^{ads} versus $E_n^{surf\ distort}$ for a large set of the larger sized $(ZnO)_n$ clusters ($n \geq 10$). For adsorption to be energetically favorable overall, the magnitude of the energy increase from distortion must be less than the energetic stabilization from adsorption (*i.e.* $E_n^{surf-distort} + E_n^{ads(ads)} < 0$). This is true for all data points in Fig. 5 as they are below the grey line defined by $E_n^{surf-distort} +$

$E_n^{ads(ads)} = 0$. The data also show that a relatively higher surface distortion leads to a more strongly adsorbed cluster. The 2D and 3D isomers are clearly separated into two groups: the 3D clusters undergo smaller distortions and do not benefit as much from adsorption, whereas the 2D clusters, which distort moderately more, are stabilized more significantly upon adsorption than the 3D clusters. Thus, although the 2D clusters experience greater strain (distortion, or energy cost) than 3D clusters, they are able to induce a greater increase in their adsorption strength with the surface, which leads to a relatively lower total system energy for surface-supported 2D clusters.

In Fig. 6 we show the separate variation in E_n^{ads} and $E_n^{free\ space}$ with respect to cluster size for the lowest energy 2D and 3D Ag-supported $(ZnO)_n$ clusters, where the sum of these two terms for each cluster gives $E_n^{on\ surface}$. Note that $E_n^{on\ surface}$ differs from E_n^{tot} by the constant value of E_{Ag_slab} (see above), and thus the variation in both terms is the same. For the most stable Ag-supported 3D $(ZnO)_n$ clusters, $E_n^{free\ space}$ decreases rapidly with increasing cluster size, whereas E_n^{ads} becomes less negative with increasing *n*. For the Ag-supported 2D $(ZnO)_n$ clusters, $E_n^{free\ space}$ decays slower than for the 3D case, but the 2D E_n^{ads} values stay relatively constant for all *n*. For both 2D and 3D clusters all respective energy values appear to be stabilizing for the largest three cluster sizes considered (*i.e.* *n* = 16, 20, and 24) The sum of E_n^{ads} and $E_n^{free\ space}$ (*i.e.* $E_n^{on\ surface}$) is plotted for the 2D and 3D GM clusters in Fig. 7a. In Fig. 7b we plot the difference in the $E_n^{on\ surface}$ values for the 2D and 3D GM $(ZnO)_n$ clusters for each size. Although for small sizes (~$n \leq 10$), there are strong variations in the 2D versus 3D energy difference, for larger sizes (~$n > 10$), the difference appears to be stabilizing around a value of approximately -0.035 eV/ZnO in favor of supported 2D isomers. This stabilization of $E_n^{on\ surface}$ is in line with the tendencies of both E_n^{ads} and $E_n^{free\ space}$ to level off for the largest cluster sizes (n ≥ 16) considered in Fig. 6.

The most energetically stable Ag-supported 2D structures tend to be those with a high proportion of Zn_3O_3 hexagonal rings which allow the Zn and O atoms to follow the hexagonal pattern of hollow sites on the Ag(111) surface. This adsorption mode is clearest in Figs. 2 and 3 for the 2D GM structures for sizes *n* = 3, 7, 11, 12, 15, 16, 20 and 24. Of these structures, those with sizes *n* = 12, 15, 16, 20, and 24, can all be regarded purely as cuts from an infinite single graphene-like ZnO sheet. The infinite single graphene-like ZnO hexagonal sheet has been shown in experiment to form when one monolayer (1 ML) of ZnO is deposited on the Ag(111) surface, and has a 7:8 epitaxial matching.[28] Our results thus clearly confirm that that this 2D hexagonal growth mode is energetically favored for even the very small nanoclusters. In Fig. 6 we include a black horizontal line to show the calculated adsorption energy for an

infinite 1 ML ZnO hexagonal sheet on Ag(111). All 2D GM clusters have an E_n^{ads} value below this line (*e.g.* 0.20-0.21 eV/ZnO lower for *n* = 16, 20, and 24) showing that they adsorb more strongly on the Ag(111) surface than the ZnO monolayer. In contrast to the infinite 2D sheet, the finite 2D clusters have a doubly coordinated terminating edge which interacts more strongly with the surface and, in turn, causes a slight peripheral bending of the 2D clusters towards the Ag surface (see side views of the 2D supported clusters in Fig. 3). It is this bending distortion that increases $E_n^{surf-distort}$ and lowers E_n^{ads} (see Fig. 5). Structurally, the Zn and O atoms in the 2D Ag-supported clusters lie between 2.1 and 3.5 Å above the Ag(111) surface; the smaller distance corresponds to the heights of the peripheral atoms in the clusters and the larger distance to the height of the atoms near the centre of the ZnO cluster. This height range corresponds to a distance of ±0.7 Å above and below those in the infinite Ag-supported ZnO 1ML sheet. We note that the lowest energy Ag-supported 2D $(ZnO)_n$ clusters found for *n* = 6 and *n* = 15 are particularly strongly adsorbed to the Ag(111) surface. The relatively more negative E_n^{ads} values for these two clusters are compensated by correspondingly relatively high $E_n^{free\ space}$ values and thus they do not have particularly low $E_n^{on\ surface}$ (E_n^{tot}) values.

Although the closed curved surfaces of bubble clusters are not as topologically well suited as 2D clusters for maximizing the number of atoms interacting with a surface, the lowest energy surface supported 3D $(ZnO)_n$ clusters also tend to exhibit Zn_3O_3 hexagonal matching with the Ag(111) surface. In particular this adsorption mode can be seen in the lowest energy Ag-supported 3D cluster isomers for sizes *n* = 6, 11, 12, 13, 15, 16, 20, and 24 (see Fig. 3). Smaller 3D clusters are only able to have one Zn_3O_3 hexagonal ring above a surface Ag atom (e.g. *n* = 12), whereas larger 3D clusters tend to flatten away from their open free space bubble structures to become more akin to partial double hexagonal layers with 5-6 Zn_3O_3 hexagonal rings above the Ag surface (*e.g. n* = 20 and 24). In Fig. 6 we also include a light grey line to indicate the calculated adsorption energy of the infinite 2 ML hexagonal ZnO film on Ag(111). Here we find that, indeed, the E_n^{ads} values for the Ag-supported 3D clusters rapidly approach this value with increasing cluster size. For $(ZnO)_n$ cluster sizes of *n* = 20 and 24, for example, the corresponding E_n^{ads} values are only 0.04 eV/ZnO and 0.02 eV/ZnO lower than the limiting adsorption energy value for the 2 ML ZnO hexagonal film. Unlike the case of the 2D clusters, the 3D Ag-adsorbed flattened $(ZnO)_n$ bubble clusters do not exhibit under-coordinated terminal atoms (i.e. all atoms are 3-coordinated as in an infinite hexagonal film) and thus mimic well the adsorption mode of the 2 ML infinite film.

The energy associated with monomeric growth of the $(ZnO)_n$ cluster, with respect to a smaller cluster $(ZnO)_{n-1}$, can be estimated by considering the first order energy difference between the $(ZnO)_n$ GM cluster and the sum of the $(ZnO)_{n-1}$ GM cluster and a ZnO monomer. This energy is also termed the

nucleation energy; for Ag-adsorbed GM clusters we have $E_n^{nuc\ surf} = E_{n-1}^{on\ surface} - \left(E_n^{on\ surface} + E_1^{free\ space}\right)$, and for free space GM clusters, $E_n^{nuc\ free} = E_n^{free\ space} - \left(E_{n-1}^{free\ space} + E_1^{free\ space}\right)$. In both cases, for ease of comparison, we assume the additive monomeric species to be a free space species. Both $E_n^{nuc\ surf}$ and $E_n^{nuc\ free}$ are plotted in Fig. 8 for $(ZnO)_n$ cluster sizes n = 5-16. The average nucleation energies over this size range are very comparable; $Avg(E_n^{nuc\ surf})$ = 4.63 eV and $Avg(E_n^{nuc\ free})$ = 4.57 eV. Within the cluster size range considered here, the values of $E_n^{nuc\ free}$ vary over a range of 1.68 eV, with the most significant variation occurring from n = 12-13. This behavior is due to the anomalously high "magic" energetic stability of the $(ZnO)_{12}$ highly symmetric T_h bubble cluster, which causes a large drop in $E_n^{nuc\ free}$. The $(ZnO)_{13}$ isomers formed from adding a monomer breaks the high symmetry and thus leads to a relatively reduced energetic stabilisation, and to a peak in $E_n^{nuc\ free}$. For the adsorbed clusters, the $E_n^{nuc\ surf}$ values vary by only 0.68 eV over the cluster size range considered and do not significantly change after any $n \rightarrow n+1$ increment. Thus, indicating that growth in this size range would not tend to favour any particular Ag-supported cluster isomer.

The coordinates of all lowest energy Ag(111)-supported $(ZnO)_n$ clusters found are given in the Supplementary Information.

Effect of different surfaces: Ag(100) and Ag(110)

In order to check the generality of the energy trends between 2D versus 3D supported clusters we observed, the effect of the type of surface exposed by the Ag support was investigated for a selection of $(ZnO)_n$ cluster sizes. In particular, we performed global optimization runs for $(ZnO)_n$ nanoclusters on both Ag(100) and Ag(110) for n = 6-8, and compared the results with those obtained for clusters adsorbed on Ag(111). The resulting GM atomic structures for Ag-supported $(ZnO)_n$ nanoclusters are shown in Fig. 9. As in the Ag(111) case, the results show that for Ag(100)-supported and Ag(110)-supported $(ZnO)_n$ clusters, 2D structures are the most stable. For n = 6, the GM structure on the Ag (111) and Ag(100) surface is found to be the same. On the corrugated Ag(110) surface, however, the GM $(ZnO)_6$ cluster is a different planar structure. For sizes n = 7 and 8, the GM $(ZnO)_n$ 2D structures are found to be different on each of the Ag(111), Ag(100) and Ag(110) surfaces. Clearly, although 2D clusters are energetically the most stable type of isomer in all three surface cases considered, the type of surface plays a very significant role in determining the specific structure of the supported GM cluster. In this preliminary extension of our main investigation, we cannot confirm whether hexagonal sheet-like 2D clusters will also dominate the low

energy landscape for larger sizes on Ag(110) and Ag(100), as they do for $(ZnO)_n$ supported on Ag(111). Further work in this direction is currently in progress.

Conclusions

Global optimization calculations using interatomic potentials with subsequent refinement using DFT optimizations were performed for $(ZnO)_n$ clusters, both in free space and in the presence of a Ag(111) support, for sizes n = 1-16, 20 and 24. With increasing size, although 3D bubble $(ZnO)_n$ isomers are quickly established as the most stable free space cluster type, on the Ag(111) surface, 2D $(ZnO)_n$ clusters are found to be more energetically stable for $n > 4$. Although 2D clusters are not energetically competitive with 3D bubble clusters in free space, on the Ag(111) surface this lower stability is more than compensated by the fact that 2D clusters interact more strongly with the support, thus lowering the total system energy. The relatively strong surface adsorption of the 2D GM clusters with respect to 3D clusters is due to three properties of the 2D GM clusters, which: (i) have a relatively high number of close Ag-cluster interactions, (ii) tend to form Zn_3O_3 hexagonal rings to match better the symmetry of the Ag(111) surface, (iii) readily distort to increase the interactions between their terminal 2-coordinated atoms and the Ag surface while lowering the total system energy. For the larger $(ZnO)_n$ clusters studied (including n = 16, 20, and 24) the separate energy contributions to the total energy per ZnO formula unit appear to be varying only slightly with increasing cluster size. For supported 3D clusters this is due to the formation of flattened bubble clusters which mimic well the adsorption mode of an infinite double hexagonal layer. For the supported 2D GM clusters the most stable isomers found can structurally be regarded as cuts from the Ag(111)-supported 1 ML hexagonal ZnO sheet known from experiment. In this way our work provides a link between the supported ZnO monomer and the supported single ZnO monolayer.

Acknowledgements

S.T.B. acknowledges support from a Spanish Government grant (MAT2012-30924) and Generalitat de Catalunya grants (2014SGR97 and XRQTC). S.M.W. acknowledges support from UK's funding agency, EPSRC (grant number EP/I03014X). We are also grateful for funding obtained from the Royal Society under their International Joint Projects 2009/R3 scheme, the Thomas Young Centre's Junior Research

Fellowship Scheme, and the COST Action CM1104 that helped establish the collaborative project between the co-authors based in London and Barcelona.

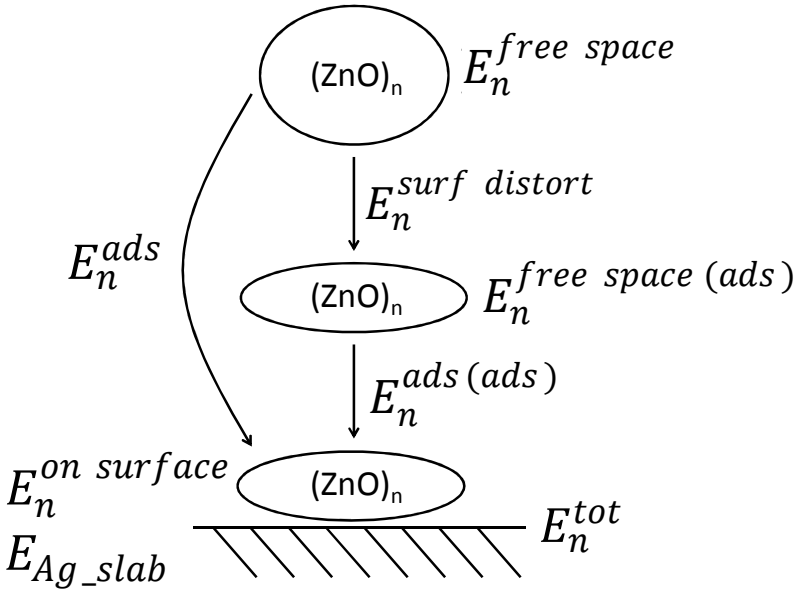

Fig. 1 Graphical representation of the meanings of the energy terms referred to in the text and the relations between them.

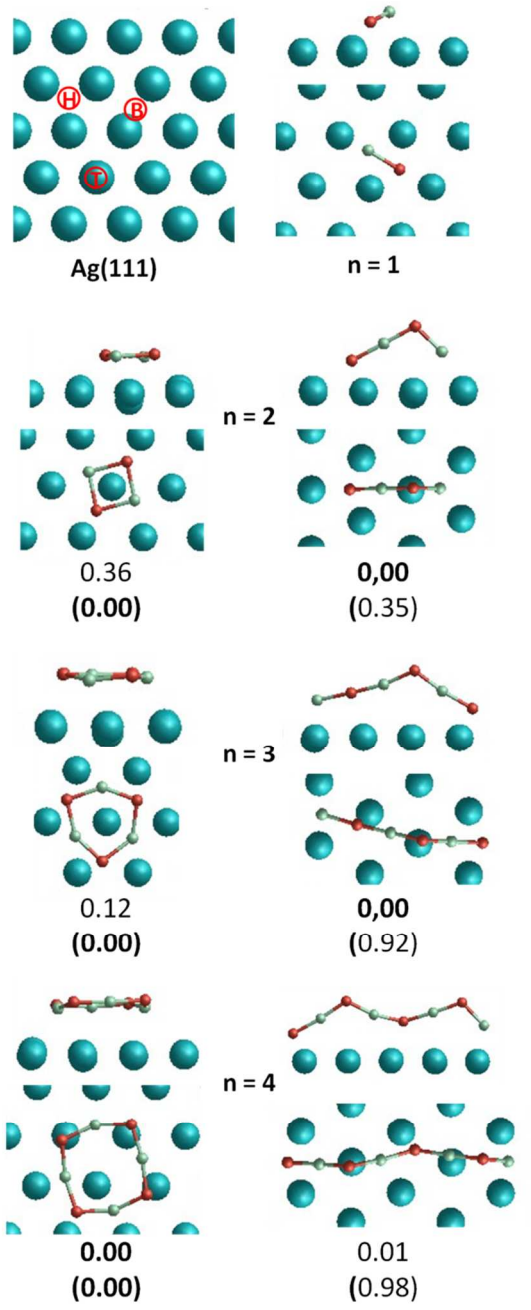

Fig. 2. Structures of stick and ring Ag(111)-supported $(ZnO)_n$ isomers for $n = 1$-4. Energies (eV/ZnO) relative to the GM Ag-supported cluster isomer are given immediately below each figure. Energies (eV/ZnO) in parentheses relate to the same cluster isomers relaxed in free space relative to the free space GM isomer. GM energies (bold) are set to zero. The top left figure shows the locations of the top (T), bridge (B) and hollow (H) sites on the Ag(111) surface.

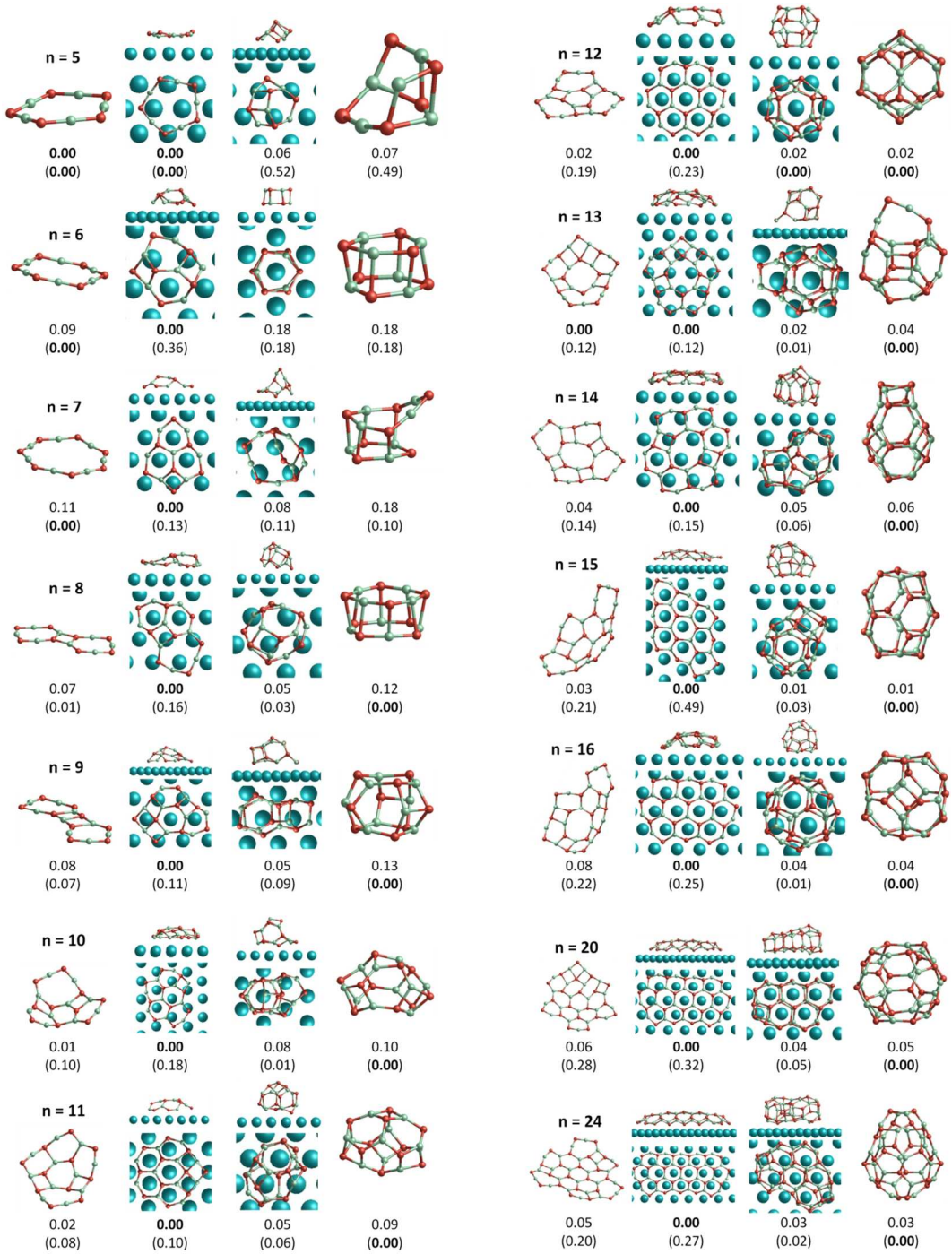

Fig. 3. Structures of lowest energy 2D and 3D $(ZnO)_n$ isomers for n = 5-16, 20, and 24: (i) in free space (far left and far right in each figure) and, (ii) Ag(111)-supported (central left and central right in each figure). Values immediately below all cluster isomers relate to the energies (eV/ZnO) of each respective cluster when on the Ag(111) support relative to that of the the GM Ag-supported cluster isomer (set to zero and marked in bold). Values in parentheses relate to the energies (eV/ZnO) of each respective cluster when relaxed in free space relative to that of the GM free space isomer (set to zero and marked in bold).

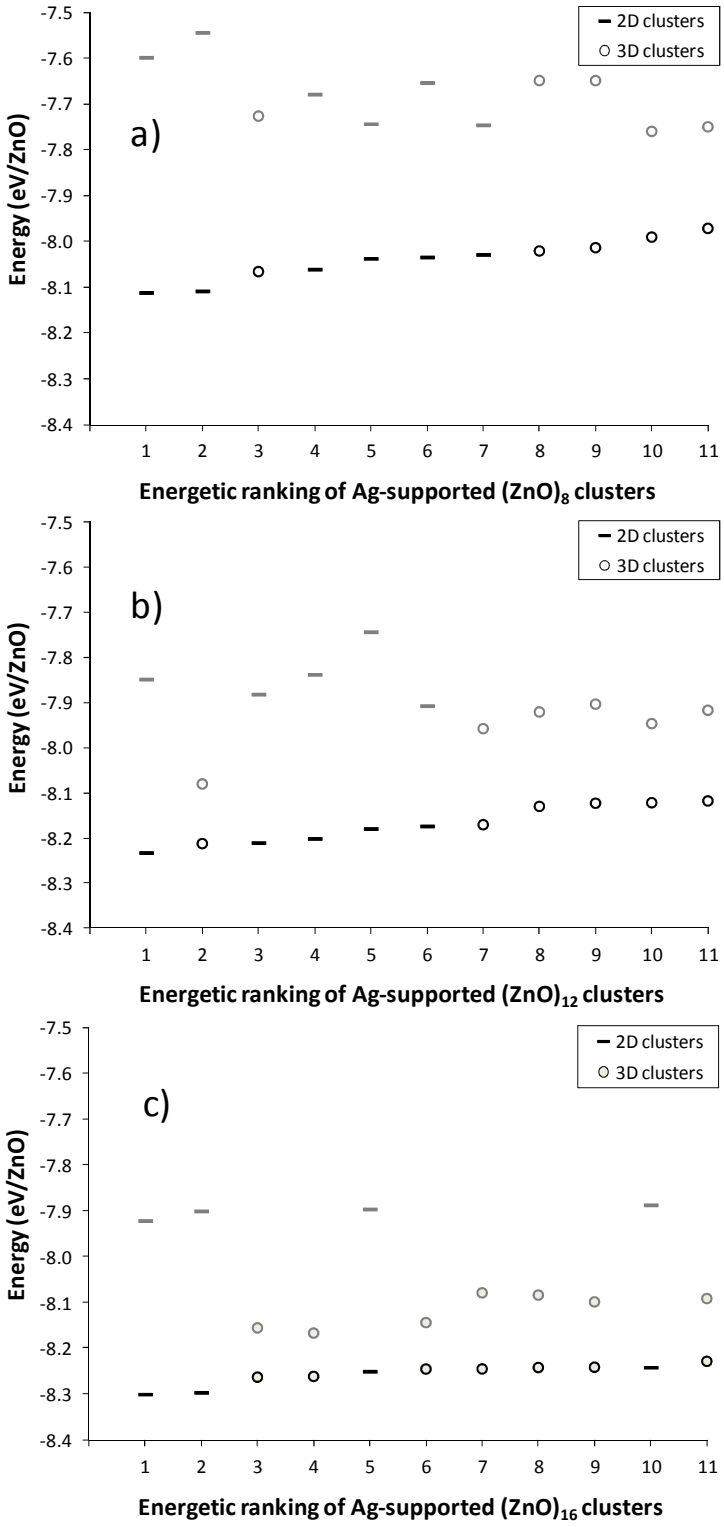

Fig. 4. Plots of $E_n^{free\ space}$ (grey data points) and $E_n^{on\ surface}$ (black data points) for the eleven $(ZnO)_n$ cluster isomers found with the lowest (*i.e.* most negative) $E_n^{on\ surface}$ values for cluster sizes *n* = 8 (a), 12 (b) and 16 (c).

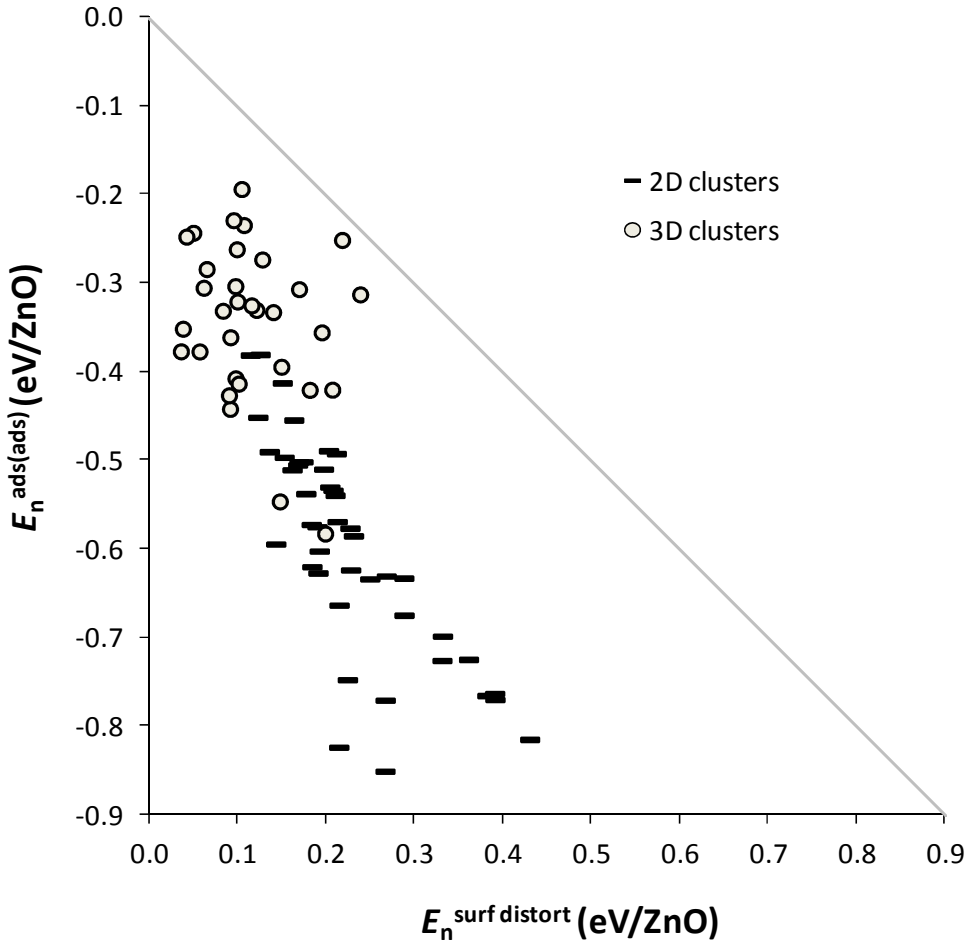

Fig. 5. Plot of E_n^{ads} versus $E_n^{surf\ distort}$ for a large set of $(ZnO)_n$ clusters for $n \geq 10$. The grey line is defined by $E_n^{surf-distort} = -E_n^{ads(ads)}$.

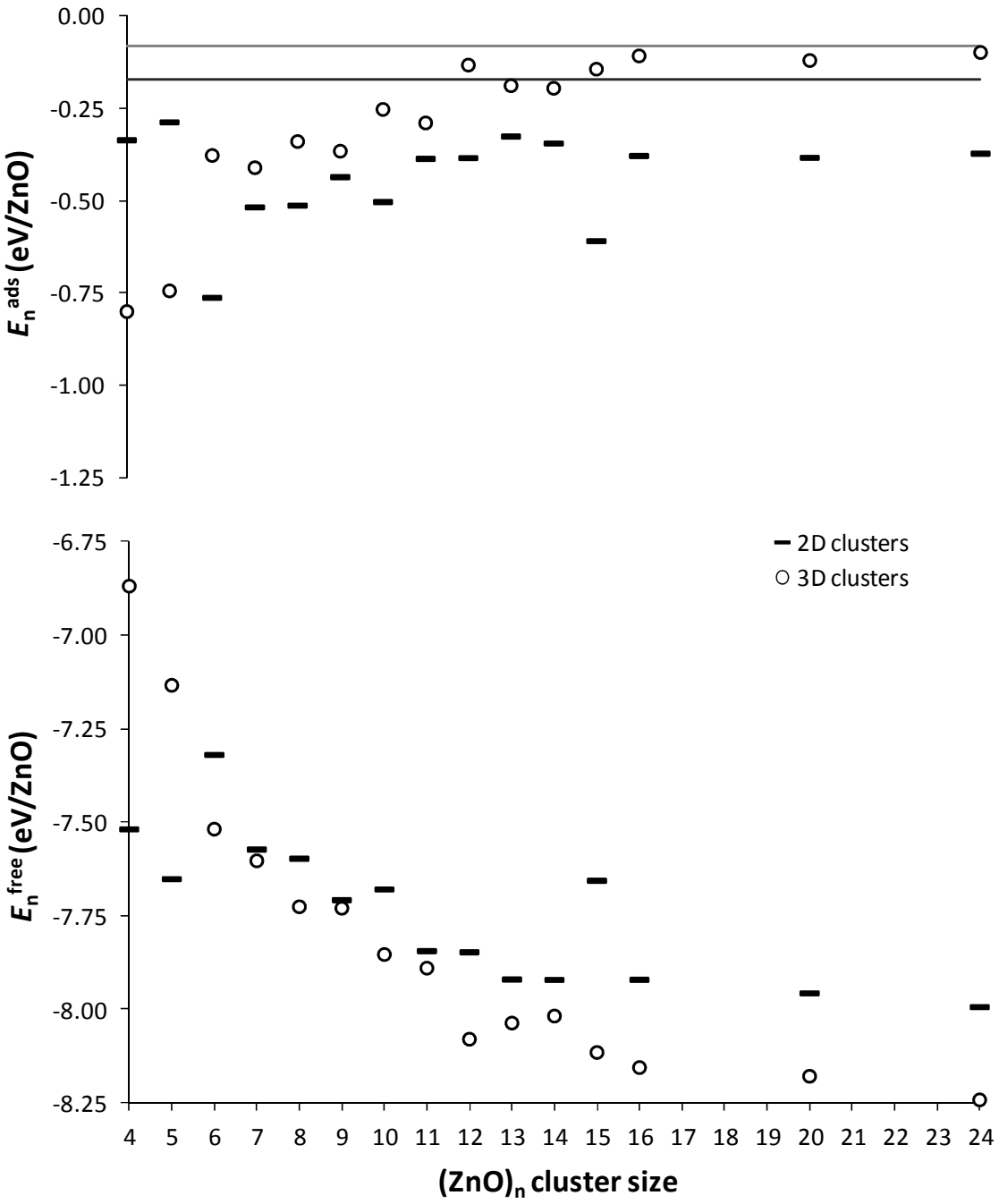

Fig. 6. E_n^{ads} (upper) and $E_n^{free\ space}$ (lower) with respect to cluster size for the lowest energy 2D and 3D Ag-supported $(ZnO)_n$ clusters for *n* = 4-16, 20, and 24. The black grey and grey horizontal lines in the upper plot show the adsorption energies of a 1 ML hexagonal sheet of ZnO and a 2 ML hexagonal bi-layer sheet of ZnO respectively.

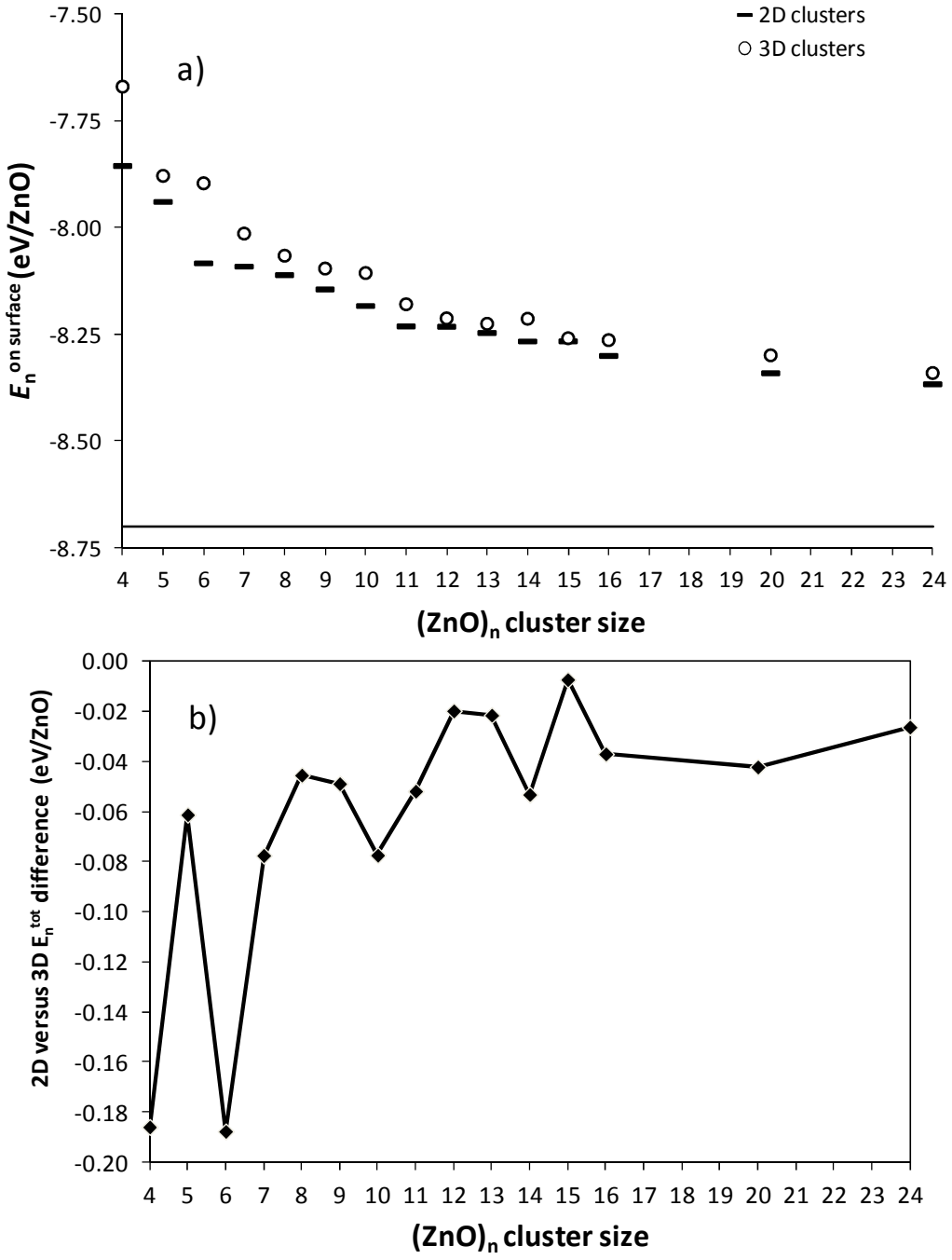

Fig. 7. a) The sum of E_n^{ads} and $E_n^{free\ space}$ (*i.e.* $E_n^{on\ surface}$) for the 2D and 3D GM Ag(111)-supported $(ZnO)_n$ clusters, for *n* = 4-16, 20, and 24. b) The difference in $E_n^{on\ surface}$ for the correspondingly sized 2D and 3D GM Ag(111)-supported $(ZnO)_n$ clusters, for *n* = 4-16, 20, and 24 (lower).

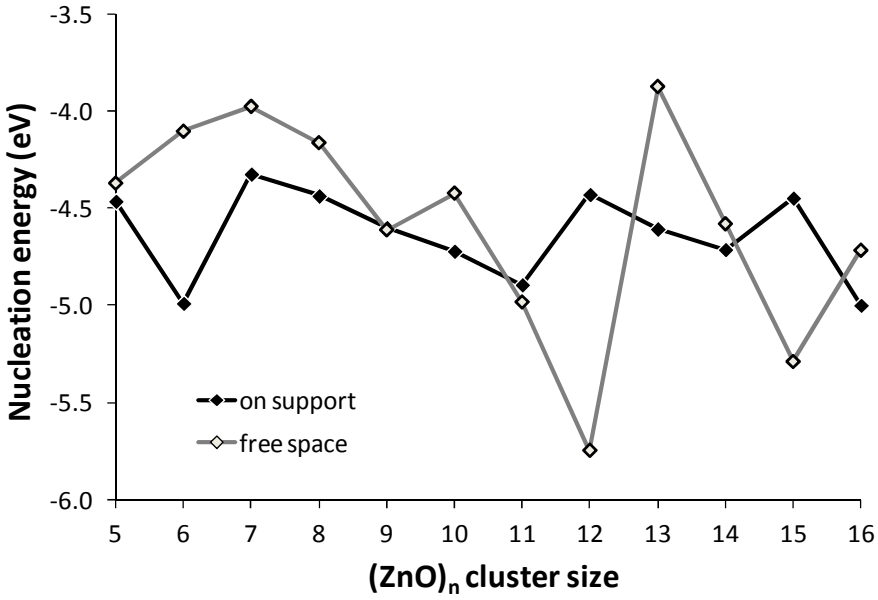

Fig. 8. $E_n^{nuc\ surf}$ and $E_n^{nuc\ free}$ for $(ZnO)_n$ cluster sizes *n* = 5-16.

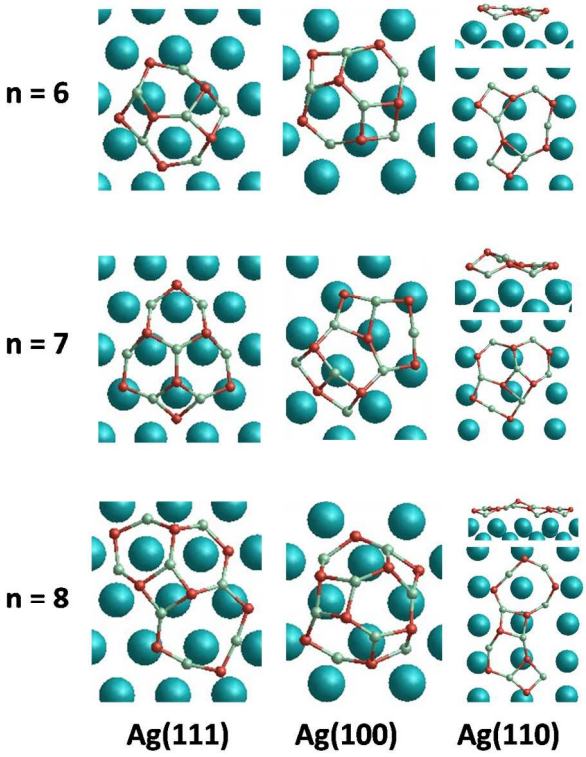

Fig. 9. Lowest energy $(ZnO)_n$ atomic structures found on the Ag(111), Ag(100) and Ag(110) surfaces for sizes *n* = 6-8.

References

[1] C. R. A. Catlow, S. T. Bromley, S. Hamad, M. Mora-Fonz, A. A. Sokol, S. M. Woodley, Phys. Chem. Chem. Phys., 2010, 12, 786.

[2] F. Baletto and R. Ferrando, Rev. Mod. Phys., 2005, 77, 371.

[3] B. Hartke, Angew. Chemie. Int. Ed., 2002, 41, 1468.

[4] B. C. Gates, Chem. Rev. 1995, 95, 511.

[5] R. Ferrando, G. Rossi, F. Nita, G. Barcaro, and A. Fortunelli, ACS Nano, 2008, 2, 1849.

[6] Lasse B. Vilhelmsen and Bjørk Hammer, Phys. Rev. Lett. 2012, 108, 126101.

[7] X. Wang, J. Song and Z. L. Wang, J. Mater. Chem. 17, 711 (2007)

[8] Behrman, E. C.; Foehrweiser, R. K.; Myers, J. R.; French, B. R.;Zandler, M. E. *Phys. Re*V.*A* 1994, *49*, R1543.

[9] J. M. Matxain, J. E. Fowler, J. M. Ugalde, *Phys. Rev.A* 2000,*62*, 053201.

[10] B. Wang, S. Nagase, J. Zhao, and G. Wang, J. Phys. Chem. C 2007, 111, 4956.

[11] A. A. Al Sunaidi, A. A. Sokol, C. R. A. Catlow, S. M Woodley, J. Phys. Chem. C, 2008, 112, 18860.

[12] I. A. Sarsari, S. J. Hashemifar and H. Salamati, J. Phys.: Condens. Matter, 2012, 24, 505502.

[13] G. Malloci, L. Chiodo, A. Rubio, A. Mattoni, *J. Phys. Chem. C*, 2012, 116, 8741.

[14] A. Michaelides, K. Reuter, M. Scheffler, J. Vac. Sci. Technol. A, 2005, 23, 1487.

[15] E. Lundgren, A. Mikkelsen, J. N. Andersen, M. Schmid, P. Varga, J. Phys. Condens. Matter, 2006, 18, R481.

[16] H. J. Glaser, Large Area Glass Coating Von Ardenne Anlagentechnik, Gmbh, 2000.

[17] J. Chen, Z. Lin, S. J. Bull, C. L. Phillips and P. D. Bristowe, J. Phys. D: Appl. Phys. 2009, 42, 214003

[18] Z. Lin, P. D. Bristowe, Phys. Rev. B, 2007, 75, 205423.

[19] C. L. Phillips and P. D. Bristowe, J. Mater. Sci., 2008, 43, 3960.

[20] D.-Y. Zhang, P.-P Wang, R.-I. Murakami, X.-P. Song. Prog. Natur. Sci.: Mater. Inter. 2011, 21, 40.

[21] Y. Dong and L. J. Brillson, J. Electron. Mater., 2008, 37, 743.

[22] J. J. BelBruno, Surf. Sci. 2008, 602, 1837.

[23] E. Sanville, J. J. BelBruno, Phys. Rev. B, 2007, 76, 085412.

[24] C. L. Phillips and P. D. Bristowe, Surf. Sci, 2011, 605, 450.

[25] J.A. Floro, J.R. Michael, L.N. Brewer, and J.W.P. Hsu, J. Mater. Res., 2010, 25, 1352.

[26] C. Gu, C. Cheng, H. Huang, T. Wong, N. Wang, T-Y. Zhang, Cryst. Grow Design, 2009, 9, 3278.

[27] K. Schouteden, Y-J. Zeng, K. Lauwaet, C. P. Romero, B. Goris, S. Bals, G. van Tendeloo, P. Lievens and C. van Haesendonck, Nanoscale, 2013, 5, 3757.

[28] C. Tusche, H. L. Meyerheim, J. Kirschner, Phys. Rev. Lett. 2007, 99, 026102.

[29] C. L. Freeman, F. Claeyssens, N. L. Allan, J. H. Harding, Phys. Rev. Lett. 2006, 96, 066102.

[30] I. Demirolgu, D. Stradi, F. Illas and S. T. Bromley, J. Phys. Condens. Mater. 23, 334215 (2011).

[31] L. Whitmore, A. A. Sokol, C. R. A. Catlow, Surf. Sci. 2002, 498, 135.

[32] I. Demiroglu, D. Stradi, F. Illas, S. T. Bromley, J. Phys.: Condens. Matter, 2011, 23, 334215.

[33] Z. Li and H. A. Scheraga, Proc. Natl. Acad. Sci. U.S.A. 84, 6611 (1987).

[34] S. M. Woodley, J. Phys. Chem. C. 2013, 117, 24003.

[35] M. R. Farrow, Y. Chow, S. M. Woodley, Phys. Chem. Chem. Phys., 2014, DOI: 10.1039/C4CP01825G

[36] D. E. E. Deacon-Smith, D. O. Scanlon, C. R. A. Catlow, A. A. Sokol, S. M. Woodley, Adv. Mater., 2014

[37] J. D. Gale, A. L. Rohl, Mol. Simul. 2003, 29, 291.

[38] J. P. Perdew, Y. Wang, Phys. Rev. B, 1992, 45, 13244.

[39] G. Kresse, J. Hafner, Phys. Rev. B, 1993, 47, 558.

[40] P. E. Blöchl, Phys. Rev. B, 1994, 50, 17953.

[41] G. Kresse, D. Joubert, Phys. Rev. B, 1999, 59, 1758.

[42] Y. Wang, W. Wang, K. Fan, J. Deng, Surface Science, 2001, 490, 125

[43] M. E. Straumanis, S. M. Riad, J. Mater. Sci. 1988, 23, 757.

[44] G. Barcaro, I. O. Thomas, A. Fortunelli, J. Chem. Phys., 132, 124703 (2010).

[45] Mercurio G, McNellis E R, Martin I, Hagen S, Leyssner F, Soubatch, Meyer J, Wolf M, Tegeder P, Tautz F S and Reuter K, 2010 Phys. Rev. Lett. 104 036102

[46] Müller F, Hüfner S, Sachdev H, Laskowski R, Blaha P and Schwarz K, 2010 Phys. Rev. B 82 113406

[47] Laskowski R, Blaha P and Schwarz K, 2008 Phys. Rev. B 78 045409

[48] A. C. Reber, S. N. Khanna, J. S. Hunjan, M. R. Beltran, Eur. Phys. J. D 2007, 43, 221.

[49] J. Heinzelmann, A. Koop, S. Proch, G. F. Gantefor, R. Łazarski and M. Sierka, J. Phys. Chem. Lett. 2014, 5, 2642.

[50] S. M. Woodley, M. B. Watkins, A. A. Sokol, S. A. Shevlin and C. R. A. Catlow, Phys. Chem. Chem. Phys., 2009,11, 3176,

[51] J. Carrasco, F. Illas and S. T. Bromley, Phys. Rev. Lett. 2007, 99, 235502.

[52] C. R. A. Catlow, S. A. French, A. A. Sokol, A. A. Al-Sunaidi, S. M. Woodley, J. Comput. Chem., 2008, 29, 2234.

[53] Atoms in Molecules: A Quantum Theory, R. F. W. Bader, Oxford University Press, Oxford, 1990